Detection of Intraseasonal Large-Scale Heat Waves: Characteristics and Historical Trends during the Sahelian Spring

J. BARBIER, F. GUICHARD, D. BOUNIOL, F. COUVREUX, AND R. ROEHRIG

Centre National de Recherches Météorologiques (UMR 3589 CNRS and Météo-France), Toulouse, France

(Manuscript received 13 April 2017, in final form 13 September 2017)

ABSTRACT

In the Sahel very high temperatures prevail in spring, but little is known about heat waves in this region at that time of year. This study documents Sahelian heat waves with a new methodology that allows selecting heat waves at specific spatiotemporal scales and can be used in other parts of the world. It is applied separately to daily maximum and minimum temperatures, as they lead to the identification of distinct events. Synoptic–intraseasonal Sahelian heat waves are characterized from March to July over the period 1950–2012 with the Berkeley Earth Surface Temperature (BEST) gridded dataset. Morphological and temperature-related characteristics of the selected heat waves are presented. From March to July, the further into the season, the shorter and the less frequent the heat waves become. From 1950 to 2012, these synoptic–intraseasonal heat waves do not tend to be more frequent; however, they become warmer, and this trend follows the Sahelian climatic trend. Compared to other commonly used indices, the present index tends to select heat waves with more uniform intensities. This comparison of indices also underlined the importance of the heat index definition on the estimated climatic heat wave trends in a changing climate. Finally, heat waves were identified with data from three meteorological reanalyses: ERA-Interim, MERRA, and NCEP-2. The spreads in temperature variabilities, seasonal cycles, and trends among reanalyses lead to differences in the characteristics, interannual variability, and climatic trends of heat waves, with fewer departures from BEST for ERA-Interim.

1. Introduction

From April to June, the subtropical Sahelian region experiences very high temperature during both nighttime and daytime, when monthly mean temperatures can range up to 30° and 40°C respectively. Furthermore, regional warming over the Sahel during the past 60 years has reached +1.5°C over the April–May period (Guichard et al. 2015). In April 2010, a huge heat wave hit the Sahel resulting in numerous deaths, mostly among children and the elderly (Azongo et al. 2012; Diboulo et al. 2012). According to Mora et al. (2017), the Sahel is exposed to deadly temperature conditions around one-third of the year, making it one of the regions with the most severe temperature conditions. The risk of these temperature hazards is enhanced by the fact that the Sahelian population is increasing very quickly: Nigeria should become the third largest country in the world by 2050, reaching 410 million, and by 2100 the population of Niger is projected to increase by at least a factor of 9, from 21 million in 2017 to 192 million in 2100 (Garenne 2016; United Nations Department of Economic and Social Affairs: Population Division 2017). Superimposed on this hot climate, heat wave events in this region at this time of the year may have particularly severe impacts on health, and also potentially on ecosystems, transportation, or agriculture (Sheehy et al. 2005; Sultan et al. 2013).

Impactful heat waves have been reported across the globe, from Chicago in 1995 to southeastern Australia in 2009. Western Europe suffered heavy human losses during the 2003 heat wave event to which 70 000 deaths are attributed (Coumou and Rahmstorf 2012); Russia's death toll reached more than 50 000 during the 2010 heat wave (McMichael and Lindgren 2011). In recent years, these events led to an increasing number of studies on how to define, characterize, understand, and predict heat waves. Because of climatic trends toward higher temperatures, their observed and future changes were also discussed: heat waves are expected to be more frequent, longer, and hotter, and cover a larger area (Cowan et al. 2014; Russo et al. 2014; Schoetter et al. 2015). Climate and heat wave temperature trends do not

Corresponding author: J. Barbier, jessica.barbier@meteo.fr

DOI: 10.1175/JCLI-D-17-0244.1

necessarily increase at the same rate: in their analysis of the heat waves in a changing climate, Gershunov and Guirguis (2012) pointed out that the ratio between the temperature mean and extremes of California's inlands decreased over the period 1850–2010. In this case, the climatic trend is thus stronger than the heat wave trend. Argüeso et al. (2016) showed that the climatic change in temperature variability has a major influence on the heat wave changes over some parts of Europe and the United States. However, they also emphasize that this finding is not valid in tropical regions where the mean seasonal warming explains most of these changes.

To date, most climatological heat wave studies have focused on Europe (e.g., Meehl and Tebaldi 2004; Fischer and Schär 2010; Stefanon et al. 2012; Schoetter et al. 2015), Australia (e.g., Perkins et al. 2012; Nairn and Fawcett 2013; Perkins and Alexander 2013; Cowan et al. 2014), the United States (e.g., Robinson 2001; Meehl and Tebaldi 2004; Gershunov and Guirguis 2012; Mutiibwa et al. 2015), or Asia (e.g., Ito et al. 2013; Lee and Lee 2016) while only very few concern the Sahel (e.g., Fontaine et al. 2013; Déqué et al. 2017). Some studies assess heat waves from a global perspective; however, they often do not show any results for West Africa (Zhang et al. 2011; Russo et al. 2014), partly because of the scarcity of in situ observations. Thus Sahelian heat waves still need to be further documented and explained; the present paper addresses this overall objective.

To be able to identify meteorological situations associated with such events, the first question that arises is how to define and detect a heat wave. A heat wave generally corresponds to a prolonged period of particularly high or extreme temperatures. The Expert Team on Climate Change Detection and Indices (ETCCDI) published a list of core indices (http://etccdi.pacificclimate.org/list_27_indices.shtml) to measure temperature extremes based on a single characteristic, for instance a frequency of occurrence of warm nights or an intensity of the maximum daily maximum temperature across the year. Every metric is relevant to particular applications. Other studies make use of indices that detect "heat wave objects" in space and time, and analyze the characteristics of these objects. Each of these studies generally develops its own specific definition. However, as highlighted by Perkins (2015), these definitions have some common features: temperature is always used in a raw or processed form, most of the times combined with a percentile-type threshold, and a minimum duration of the heat wave is often considered. Most studies use the daily maximum temperature (Fischer and Schär 2010; Stefanon et al. 2012; Schoetter et al. 2015) or separately analyze daily minimum and maximum temperatures, hereafter referred to as Tmin and Tmax (Gershunov and Guirguis 2012; Perkins et al. 2012; Fontaine et al. 2013; Perkins and Alexander 2013; Mutiibwa et al. 2015). Robinson (2001) and Willett and Sherwood (2012) use a heat index accounting for both temperature and humidity effects (respectively relative humidity and vapor pressure). The vast majority of the studies use a percentile, very often the 90th percentile, as the lower limit over a moving time window. By design, the methods using a moving time window detect heat waves throughout the year in a uniform way. The minimum duration of heat waves is also often defined to be 3 days.

In this study, we will define a heat index that follows the basic metrics described above in order to identify Sahelian heat waves from March to July (i.e., during the hottest months of the year). We also aim at defining Sahelian heat waves as large-scale meteorological events, coherent in space and time, arising as strong and rapid departures of temperature at synoptic–intraseasonal scales. We then predominantly focus on meteorological scales rather than other signals such as interannual fluctuations, annual cycles and climatic trends. In other words, as in Gershunov and Guirguis (2012) and Stefanon et al. (2012), we consider heat waves as occurring in a nonstationary climate. One more motivation to remove the climatic trends is that thresholds based directly on temperatures are expected to be exceeded more often due to the mean climatic warming. The heat wave detection is based either on Tmax or Tmin because processes controlling daytime and nighttime temperatures in the Sahel are likely to be distinct: for instance, maximum temperature is often influenced by the incoming surface shortwave radiation whereas the minimum temperature is very sensitive to the amount of water vapor during this time of the year (Guichard et al. 2009; Slingo et al. 2009; Gounou et al. 2012; Largeron et al. 2017, manuscript submitted to *Climate Dyn.*). Another noteworthy difference for this heat index is that the percentile is fixed over the whole March–July period instead of over a moving window: it enables a seasonal analysis of the heat wave occurrence. Although large-scale atmospheric phenomena or modes of climatic variability are not studied in this paper, our results should be valuable for further studies addressing this topic, in the Sahel as well as in other regions.

The methodology used to build our heat index and to study meteorological heat waves over the Sahel in spring is explained in section 2. Section 3 presents the climatological characteristics of these heat waves, including their frequency, duration, intensity, and spatial extent. Benefits and limits of the present heat wave definition are further discussed in section 4, via a comparison with other definitions. An assessment of the sensitivity of the results across different temperature datasets (including three meteorological reanalyses) is also presented. Finally,

section 5 emphasizes the evolution of heat wave properties over the recent historical period and compares it to regional warming. Conclusions are given in section 6.

2. Datasets and methodology

a. Datasets

We use daily minimum and maximum temperature datasets provided by one observationally based gridded product and retrieved from three meteorological reanalyses over 0°–40°N, 20°W–40°E, hereinafter referred to as the African domain. These datasets are the following:

- The Berkeley Earth Surface Temperature (BEST; Rohde et al. 2013a,b), which provides data on a 1° × 1° grid from 1880 until recent years. We consider the period 1950–2012 because observations in the Sahel are very sparse prior to 1950.
- The European Centre for Medium-Range Weather Forecasts (ECMWF) interim reanalysis (ERA-Interim; Dee et al. 2011) over 1979–2012 on a 1° × 1° grid.
- The National Centers for Environmental Prediction (NCEP)–U.S. Department of Energy (DOE) AMIP-II reanalysis (NCEP-2; Kanamitsu et al. 2002) over 1979–2012 on a 2° × 2° grid.
- The Modern-Era Retrospective Analysis for Research and Applications (MERRA; Rienecker et al. 2011) from the National Aeronautics and Space Administration's Global Modeling and Assimilation Office over 1979–2012 on a 0.5° × 0.66° grid.

The use of several datasets is motivated by the fact that data are sparse in the Sahel. The Berkeley Earth website provides historical values of the number of stations used in their dataset at regional, national, and local scales. For instance, in Mali (http://berkeleyearth.lbl.gov/regions/mali), around 10 stations from inside the country and 100 stations from neighborhood regions are used. The numbers of stations used are not constant in time, with fewer stations prior to 1950. Thus the influences of distinct physical parameterizations and assimilation procedures in the three reanalyses, as well as the interpolation method used in BEST, are all likely to induce differences in surface temperatures. The main differences are documented in the appendix and briefly summarized below.

BEST and the three reanalyses were compared over 1979–2010 to two surface synoptic observation (SYNOP) stations with consistent long-time temperature series: Hombori, Mali (15.33°N, 1.8°E) (Guichard et al. 2015; see Fig. A1 in the appendix), and Niamey, Niger (13.48°N, 2.17°W) (Leauthaud et al. 2017; not shown). Observations from both stations are included in BEST, but the time series of Hombori used by BEST has many gaps, especially over the recent years. The dataset we used was enhanced and quality checked by Mougin and collaborators from the Mali Meteorological Agency from paper archives (Guichard et al. 2015). In addition, BEST, ERA-Interim, NCEP-2, and MERRA were compared over 10°–20°N, 10°W–20°E, hereinafter referred to as the Sahelian domain (Fig. A2). Numerous differences are found between datasets; their magnitudes fluctuate from month to month. As may be expected from its construction, BEST is the closest to these two SYNOP stations in terms of monthly and seasonal mean. BEST is constructed by kriging (interpolating) in situ data, notably including SYNOP stations. Away from the observations, BEST might be less accurate. On average, in NCEP-2 Tmax and Tmin are both too low (e.g., by more than 3°C in April for Tmin), whereas Tmax is too high in MERRA and too low in ERA-Interim (Figs. A1a and A2a). In NCEP-2, the seasonal cycle is shifted by about one month (Figs. A1b and A2b) and the Tmin variance is largely overestimated (Figs. A1c and A2c). The Tmax variance is generally higher in the three reanalyses than in BEST, without any clear link between the grid size of the reanalysis and the magnitude of the variance (Figs. A1c and A2c). The distributions are most of the time skewed to the left, especially for Tmax in April and May (Figs. A1d and A2d): this negative skewness highlights the predominance of time sequences of relatively similar warmer days, interrupted by less frequent but much cooler days. It also suggests that physical and dynamical mechanisms constrain Tmax upper extrema.

Following these comparisons, BEST is hereinafter set as the reference. Furthermore, its historical depth, going back to 1950, enables trend computation over longer time periods than 1979–2012. Differences between the various databases go further than a mean shift, and therefore one may expect differences between detected heat waves (see section 4b).

b. Heat wave detection

Temperature fluctuates at climatic, multidecadal, and annual time scales as well as at intraseasonal and synoptic scales, and also within the diurnal cycle. We focus on heat waves corresponding to intraseasonal fluctuations of temperature, which can be defined as strong and rapid temperature departures from its annual cycle.

Following approaches that are commonly used to detect and document the synoptic and intraseasonal variability of the West African monsoon (Janicot et al. 2011; Roehrig et al. 2011; Poan et al. 2013), our heat wave detection is based on temperature anomalies from the slow variations of the annual cycle—variations that are

modulated by interannual, multidecadal, or longer-term variabilities. These anomalies are computed using a 90-day high-pass spectral filter applied on the 1950–2012 temperature time series. A spectral analysis of Tmin and Tmax time series over the Sahelian domain (not shown) revealed three peaks of energy at the periods 365, 185, and 123 days, consistent with the shape of the mean annual cycle over the region having two maxima, one in spring and one in autumn in relation with the annual cycle of the insolation and monsoon precipitation (Guichard et al. 2009). The 90-day filter allows removing the annual cycle of temperature, as well as its modulation at longer time scales. The diurnal cycle is dealt with by studying maximum and minimum temperatures separately.

The heat wave detection includes four distinct operations: 1) a filtering of the low frequencies; 2) a selection of the strongest temperature anomalies; 3) a removal of the short-lived, small, and scattered heat waves because we want to focus on relatively large-scale events; and 4) a geographical selection of the heat waves by keeping only those found in the Sahel. The different steps are detailed below and illustrated with the results obtained for the year 1992 with Tmax at a grid point roughly located at the center of the Sahelian domain (Fig. 1).

1) Filtering: At each grid point on the African domain for the total period, Tmax and Tmin anomalies are computed using a 90-day high-pass filter (Figs. 1a,b).
2) Selection of hottest days: For each grid point, a day is considered ''hot'' if the local temperature anomaly exceeds the 90th percentile of the distribution over 1950–2010 for March–July (red shading). Such days are identified with a binary heat index (depicted by red dots in Fig. 1c).
3) Removal of small and short heat waves: This is done via the sequential application of spatial and temporal constraints. The running order of the spatiotemporal constraint matters, as emphasized by Schoetter et al. (2015). Here, we chose to apply the spatial constraint before the temporal one as this is more suitable for studying propagating heat waves.
   (i) Spatial constraint: A connectedness constraint based on a region growing technique (Petrou and Bosdogianni 2004; Fiolleau and Roca 2013) is applied to identify and label each connected element, which is discarded when its area covers less than $60 \times 10^4\,\mathrm{km}^2$. This constraint removes numerous small-scale events. This surface threshold corresponds to approximately 20% of the Sahelian domain. For each day, the occurrence of a heat wave in the Sahelian domain is indicated by a black dot in Fig. 1d.
   (ii) Temporal constraint: The minimum duration of the heat waves is set to 3 days. The impact of this constraint is illustrated in Fig. 1e with several heat waves removed in July and a few in March, May, and June (cf. Figs. 1d and 1e).
4) Sahel domain selection: Finally, we only keep heat waves occurring over the Sahelian domain via the labeling done by the connectedness constraint (Fig. 1f) and define the month a heat wave belongs to by its median date. An example of the spatial structure and time evolution of a detected heat wave is given at the bottom of Fig. 1.

The final binary heat wave index is called HImax (HImin) for Tmax (Tmin), while the heat waves finally detected are generically referred to as HWmax (HWmin). The results are not very sensitive to small changes in the prescribed criteria (not shown). Note that this methodology can be applied to any region in the world simply by changing the selected domain on the final step.

The spatial constraint corresponds to approximately 2.5% of the large African domain, and for both heat wave types, 55% of all the March–July periods studied from 1950–2012 were affected. In other words, an HWmax (HWmin) event happens every two days on average somewhere in Africa. In theory, there can be more than one heat wave simultaneously present in different regions on a given day. In practice, over the African domain, around 20% of heat wave days are affected by two geographically distinct heat waves, and around 2.5% by three or more events. The numbers of time-overlapping heat waves are reduced substantially when selecting heat waves over the smaller Sahelian domain: among the total number of days during which a heat wave was present (1007 days for HWmax and 871 for HWmin), only a very few of them were affected by two heat waves (7 for HWmax and 4 for HWmin).

c. *Other heat wave indices*

To analyze the impact of the heat wave definition and to compare our results with those obtained with indices commonly found in the literature, three other heat wave indices are considered. These indices differ in the first two steps of the methodology presented above, namely the temperature filtering and the selection of the hottest days (definition of the 90th percentile).

- 15DW: Many heat wave studies use a relatively shorter moving window to compute a seasonally dependent threshold for their detection algorithm: a 5-day window (e.g., Fontaine et al. 2013; Mutiibwa et al. 2015), a 15-day window (e.g., Fischer and Schär 2010; Perkins et al. 2012; Perkins and Alexander 2013; Cowan et al. 2014),

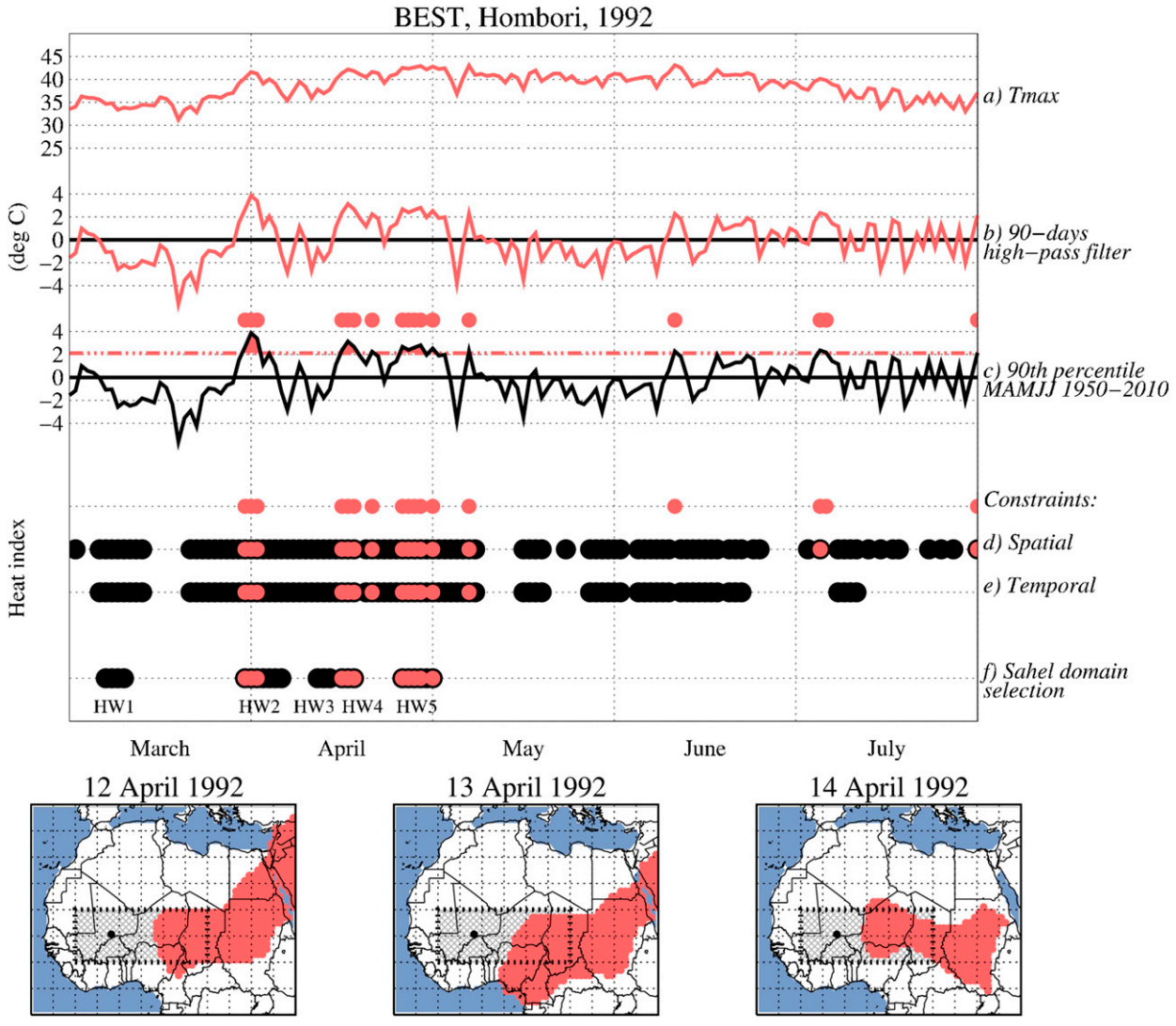

FIG. 1. Illustration of the methodology used to define the heat index using the example of the HImax in 1992 at Hombori (its geographic position is indicated with a black dot in the bottom set of panels). (top) The first three lines represent time series of (a) Tmax, (b) Tmax anomalies, and (c) with the 90th quantile superimposed (red dashed-dotted line) and the days whose temperatures exceed this quantile (red dots). The red dots indicate the detection of heat waves at Hombori, black dots the detection of heat waves within the African domain after (d) the spatial constraint and (e) the temporal constraint, and finally (f) the heat waves over the Sahelian domain. Each numbered line in (top) represents a step from the initial temperature to the final heat index. There are five heat waves in 1992 over the Sahelian domain; (bottom) the spatial extend of the third heat wave (HW3) is represented in the maps (red-colored area) and the gray hatched boxes indicate the Sahelian domain.

or a 31-day window (e.g., Russo et al. 2014). We test the impact of a 15-day moving window to define a seasonal-dependent 90th percentile instead of our constant 90th percentile. The 90-day high-pass filter is kept.

- NoFilter_15DW: As in most heat wave detection algorithms, we use unfiltered raw temperatures and a threshold based on the 90th percentile computed using a 15-day moving window centered on the current calendar day (Fischer and Schär 2010; Perkins et al. 2012; Perkins and Alexander 2013; Cowan et al. 2014).
- NoFilter: This uses raw temperatures and a fixed-percentile threshold for the whole period (March–July), as in Schoetter et al. (2015) and Ouzeau et al. (2016).

d. Heat wave metrics

Heat wave studies commonly focus on three main features: intensity, duration, and frequency (Perkins 2015), which can be computed based at the event scale or for each grid point. Here we use the event-based

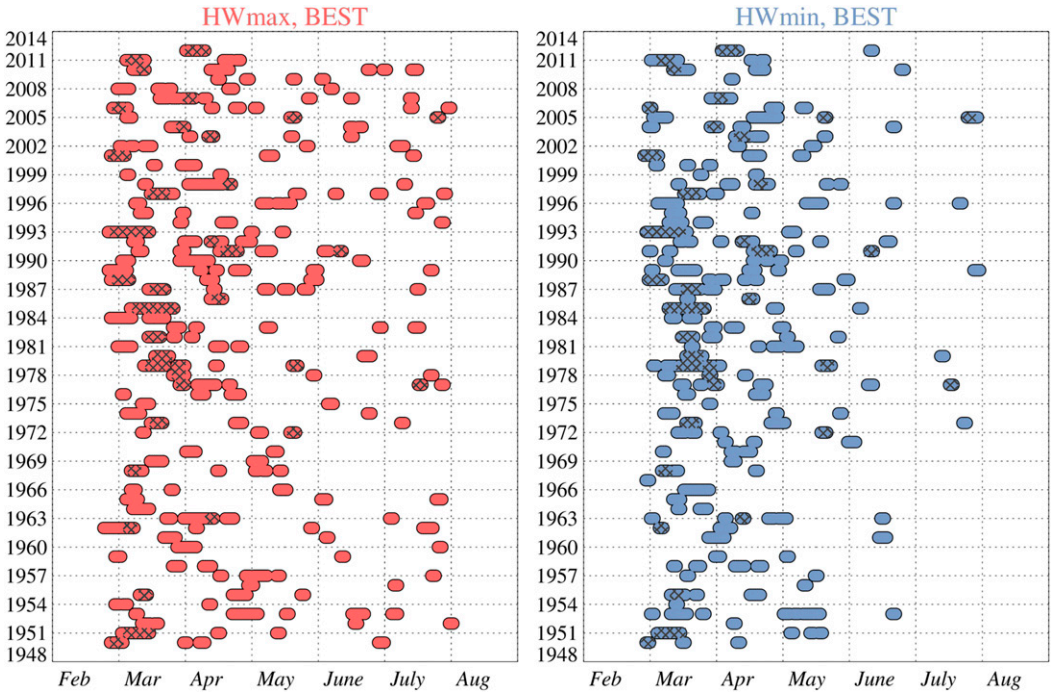

FIG. 2. Chronology of the heat waves for the heat index using (left) HWmax (red) and (right) HWmin (blue), using the BEST dataset from 1950 to 2012. Each point indicates the occurrence of a heat wave for the corresponding day and year. The hatched areas indicate heat waves that are shared by both HWmax and HWmin, cover an area of at least 20% of the Sahelian domain and last at least 3 days.

approach. We also add the spatial extension to these usual features. Besides the frequency of events per year, we grouped the features into two different types of characteristics: the first one relates to morphological properties while the other gathers the temperature-related characteristics.

Morphological characteristics are the following:

1) duration of the heat wave in days and
2) mean area covered in the Sahelian domain, expressed as a percentage relative to this domain. It is computed for each day of the heat wave and averaged over these days.

Temperature variables are the following:

1) Tmax, Tmin, and daily mean temperature Tmean, defined as Tmean = (Tmax + Tmin)/2,
2) Tmax and Tmin anomalies (i.e., the 90-day high-pass-filtered temperatures), and
3) the diurnal temperature range (DTR) = Tmax − Tmin.

Each of these variables is averaged over the heat wave space and time dimensions.

Trends of the heat waves' characteristics are computed by first averaging the heat wave characteristics each year, either over the whole period (March–July) or over the core hottest spring months (April–May). The yearly mean temperature-related characteristics of heat waves correspond to weighted averages. More precisely, for each heat wave we weighted the averaged value by the area and the duration of the heat wave so that the contribution of heat waves is proportional to their size and duration. Then a linear regression analysis of the yearly mean series is performed and the retrieved multidecadal trend is considered significant if the associated p value is lower than 0.05. For comparison with changes occurring at larger scales, climatic trends of Tmin and Tmax are computed similarly over the Sahelian domain.

3. Morphology and intensity of Sahelian heat waves

A chronology of the Sahelian heat waves detected as described in section 2 (HWmax and HWmin) is shown in Fig. 2 from March to July for the period 1950–2012. About 3.3 HWmax and 2.9 HWmin per year are detected. Only 20% of them occur simultaneously (crosses in Fig. 2), meaning that in terms of Tmin and Tmax they impact a region larger than 20% of the Sahelian domain for more than 3 consecutive days. This underlines the importance of distinguishing heat waves characterized by high Tmin from heat wave characterized by high Tmax in the Sahel. On average, HWmax events cover 42% of the Sahelian domain or $126 \times 10^4\,\mathrm{km}^2$, last 5 days, and reach a

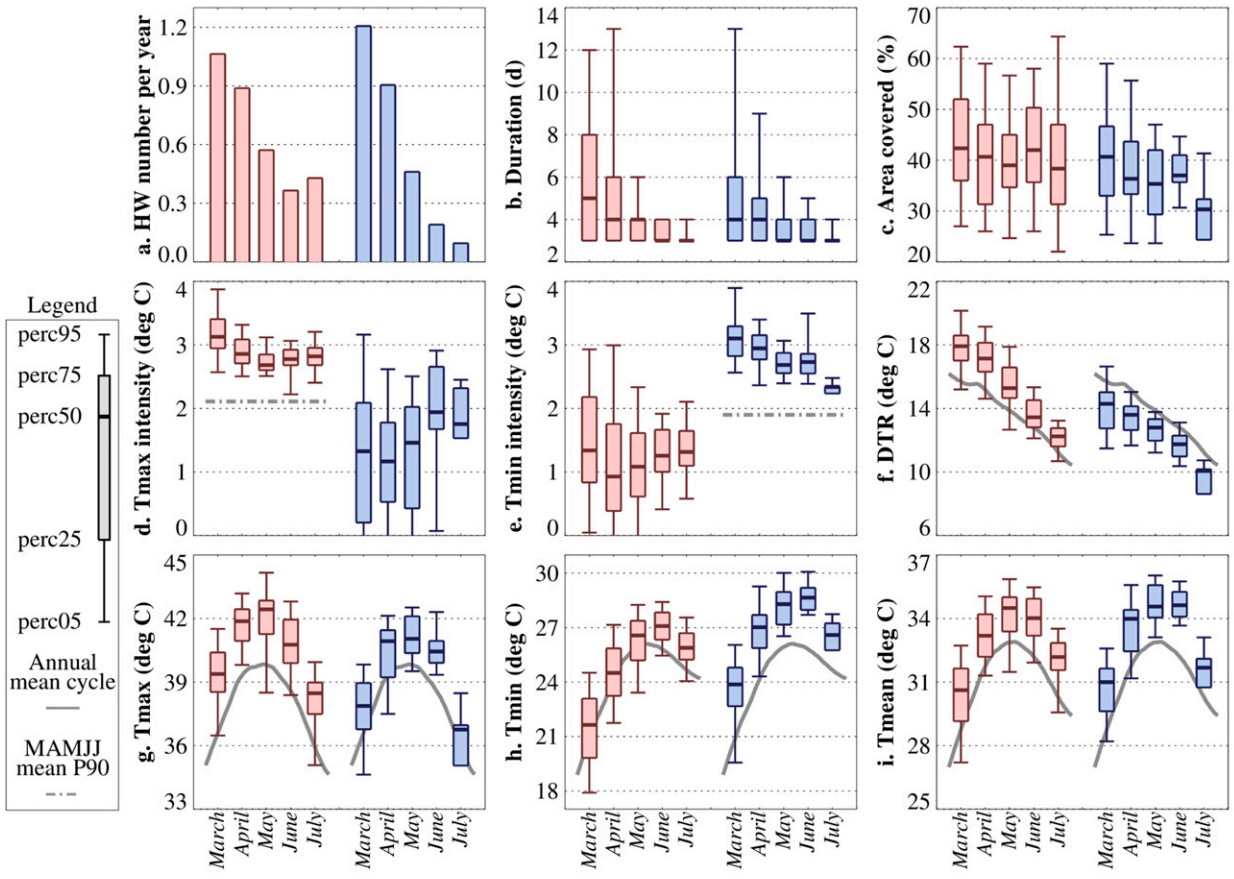

FIG. 3. Evolution of the morphological and thermodynamical characteristics of HWmax (red) and HWmin (blue) from March to July for the period 1950–2012 represented by percentile box plots: (a) number of heat waves per year, (b) duration, (c) area covered, (d) Tmax intensity, (e) Tmin intensity, (f) diurnal temperature range, (g) Tmax, (h) Tmin, and (i) Tmean. In (f)–(i) climatological values smoothed by a moving average over 21 days are shown with gray lines.

mean temperature anomaly of 3°C. HWmin have similar mean characteristics except for a slightly smaller area of $118 \times 10^4\,\mathrm{km}^2$. HWmin and HWmax events are evenly distributed across the 1950–2012 period, with no evident trend of their frequency of occurrence (see section 5 for more details) as expected from the filtering process, which notably induces a detrending of the data. Moreover, these frequencies of occurrence display a strong interannual variability, up to sixfold (see, e.g., the differences between years 1986 and 1987 for HWmax in Fig. 2).

From a seasonal point of view, the further into the season, the shorter and the less frequent the heat waves become (Figs. 2 and 3a,b). This result is consistent for both heat wave types, but slightly more pronounced for HWmin during the end of spring, in June and July. There is on average less than one HWmin every five years in these two months, whereas HWmax events are twice as frequent in this period of the year even though they are quite rare compared to early spring (Fig. 3a). In both cases, their mean temperature anomaly is also weaker than in March (Figs. 3d,e), consistent with lower variability of temperatures anomalies in June–July than in March–April (Fig. A1e and A2e).

In early spring, midlatitude synoptic disturbances, such as cold surges (Knippertz and Fink 2006; Vizy and Cook 2009) and the northward progression of the intertropical discontinuity (ITD)—which corresponds to the narrow interface at the surface between warm moist southwesterly monsoon flow and the much hotter and drier northeasterly wind from the Sahara Desert; Lélé and Lamb 2010)—strongly modulate the amplitude of surface air temperatures fluctuations over the Sahel (Largeron et al. 2017, manuscript submitted to *Climate Dyn.*). The decrease of Tmin anomalies during HWmin events further continues until July (Fig. 3e), when the ITD is generally located north of the Sahel. This is possibly related to the establishment of a steady monsoon flow, as the presence of water vapor prevents strong nighttime cooling and tends to dampen nighttime temperature fluctuations (Guichard et al. 2009; Slingo

et al. 2009). By contrast, Tmax anomalies during an HWmax (Fig. 3d) are slightly higher in June and July, around the West African monsoon onset (Ali et al. 2003; Sultan et al. 2003), than in May. This is consistent with the increasing Tmax variability during the early monsoon. Indeed, in the early monsoon phase, rain events cause sharp drops in Tmax (Guichard et al. 2009; Schwendike et al. 2010). These Tmax drops last for several days after the rain and are mainly due to jumps in surface evaporative fraction (Kohler et al. 2010; Lohou et al. 2014). Such Tmax fluctuations at that time are probably favored by heterogeneous rain events (Fitzpatrick et al. 2015) and frequent dry spells (Sivakumar 1992; Frappart et al. 2009). The impact of rain on the surface energy budget is thus likely to increase Tmax variability in the early monsoon phase.

The seasonal fluctuations of Tmax, Tmin, Tmean, and DTR averaged over HWmin and HWmax events are relatively close to their respective mean annual cycles (Figs. 3f–i). The hottest (highest Tmax) HWmax occur in May, around the Tmax annual cycle peak in April–May, with 50% of HWmax having Tmax above 42°C. Likewise, the hottest (highest Tmin) HWmin occur in June, concomitant with the Tmin annual cycle peak in May–June, with 50% of HWmin having Tmin greater than 28.5°C. Note, however, that the occurrence of HWmax (HWmin) events does not systematically imply that Tmin (Tmax) is higher than its climatic value (Figs. 3g,h). As a result, the DTR tends to be well above its climatic value during HWmax events, and well below it during HWmin (Fig. 3f). Finally, Tmax remains above the human body temperature of 37°C during the core spring months April–June for both HWmax and HWmin (Fig. 3g): above this threshold, the human body cannot dissipate heat with its environment and cool down (Basu and Samet 2002; Kovats and Hajat 2008; Mora et al. 2017). Thus, even if this detection method is not specifically designed for health impacts, the detected heat waves are expected to be dangerous for the population health.

The impact of the criteria used for the detection of heat waves can be seen in Fig. 3: the 3-day criterion strongly shapes the heat wave duration (Fig. 3b), with many only just passing this value (47% of HWmin and 44% of HWmax last 3 days). On the contrary, the detection method is qualitatively less sensitive to the spatial criterion (Fig. 3c) and to the 90th percentile threshold (Fig. 3d,e) as the two associated characteristics are far above the chosen thresholds. This indicates that Sahelian heat waves tend by essence to be large-scale events corresponding to large deviations from the mean annual cycle of temperature.

On average over March–July, heat wave characteristics are generally not very strongly coupled. However, the correlations R between Tmax and Tmin and between DTR and Tmin are significant at the 95% level, being respectively for HWmax (HWmin) 0.53 (0.78) and −0.72 (−0.55). A significant correlation between the area covered by heat waves and the duration of heat waves is also found in March: for both HWmax and HWmin, the correlation is close to 0.5. Note that over the Sahelian domain, the correlations between monthly mean values of Tmax and Tmin and between monthly mean values of DTR and Tmin are also significantly correlated for each month ($R > 0.5$). This indicates that these couplings between Tmax and Tmin and between DTR and Tmin remain valid from the smaller scale of heat wave events to monthly time scales.

As previously discussed, very few HWmax and HWmin events overlap in space and time. Nevertheless, about 20% of concomitant HWmax and HWmin events are larger than 20% of the Sahelian domain for more than 3 days. These events lead to particularly stressful periods for Sahelian societies. Such heat wave events occur about once every two years over the region, last 4.8 days on average, are slightly smaller in extent than their parent HWmin and HWmax event ($110 \times 10^4\,km^2$ vs 118 and $126 \times 10^4\,km^2$, respectively) and reach a mean value of 3.5 (3.4) °C for Tmax (Tmin) anomalies, compared with 3°C for HWmax (HWmin). Tmax (Tmin) values of the overlapping heat waves are not significantly different from the HWmax (HWmin) values at the 95% level.

4. Sensitivity of heat wave characteristics to the definition and dataset

a. *Impact of the heat wave definition*

We assess the sensitivity of our heat wave definition by comparing our results (section 3) with those obtained with definitions that are often used in the literature (section 2c). The heat wave characteristics obtained with each definition are summarized in Fig. 4 and Table 1.

The 15DW set tests the impact of taking a 15-day moving window to define a seasonally dependent temperature anomaly threshold, instead of a constant percentile over March–July. 15DW heat wave frequency of occurrence is now fairly constant throughout the season (Fig. 4a): indeed, the use of a moving window for the determination of the 90th percentile causes a fixed number of days to be extreme for each calendar day. Otherwise, other heat wave properties are not significantly modified, except for a small difference in the anomaly amplitudes (Figs. 4d,e): the temperature anomalies are now higher in March–April and then lower in June–July. This is related to the stronger temperature variability in the early months, resulting

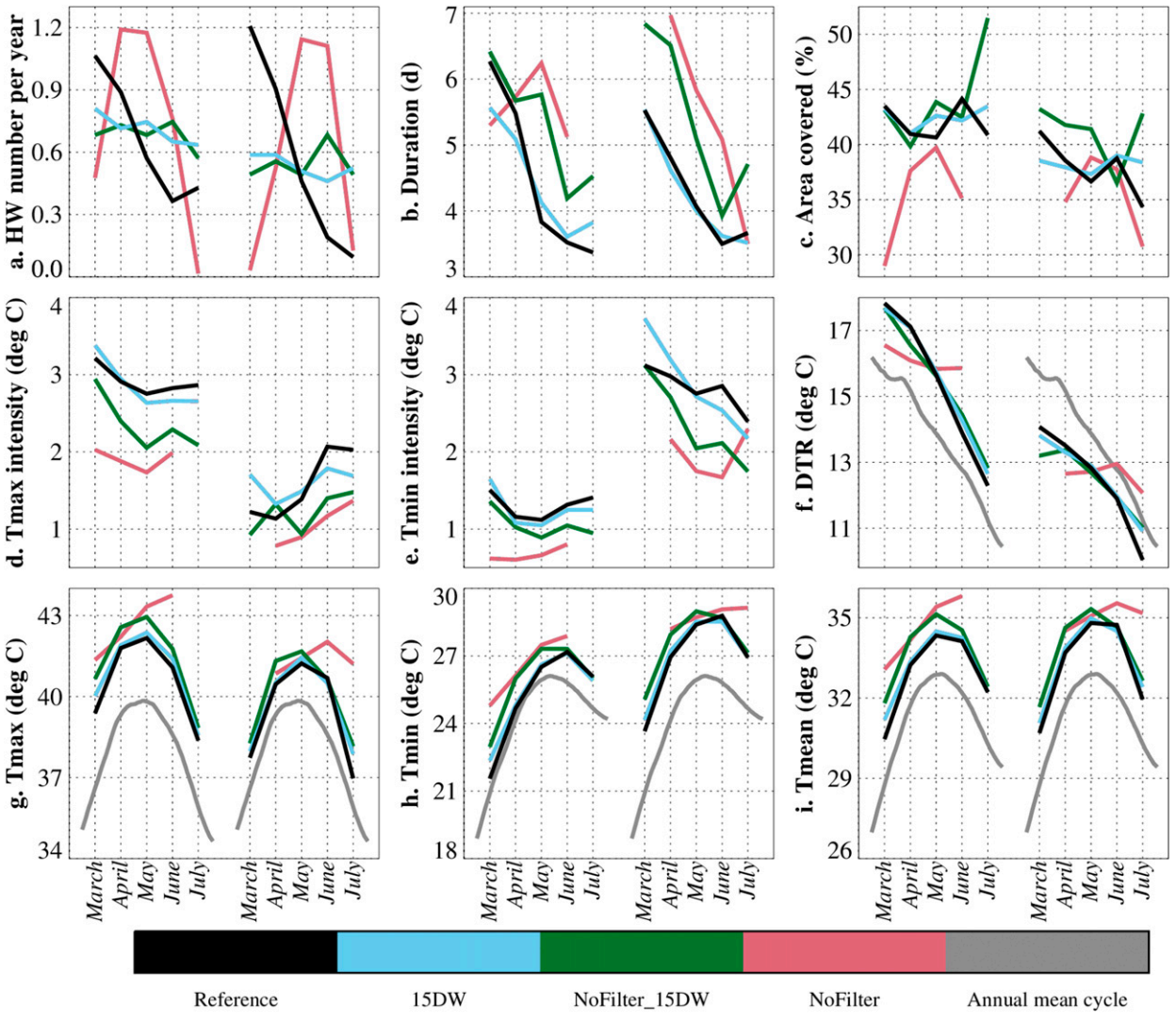

FIG. 4. As in Fig. 3, but for averaged characteristics of heat waves identified with different methodologies: Reference data (black line), 15DW (light blue line), NoFilter_15DW (green line), and NoFilter (red line). Monthly characteristics computed over less than five heat waves are not plotted. In each panel, the curves on the left-hand side refer to HWmax and those on the right-hand side to HWmin.

in more heat waves found in these months with our own definition.

The NoFilter_15DW is often used in the literature. As for 15DW, the frequency of occurrence of heat waves is almost constant throughout March–July. The NoFilter_15DW heat waves last longer, are overall larger, and their temperature anomalies are smaller, while their mean Tmax, Tmin, and Tmean are higher (Fig. 4). Finally, as for 15DW and the reference dataset, the duration of both HWmin and HWmax also decreases markedly from March to June.

The NoFilter heat wave set is mainly driven by the annual temperature cycle and most heat waves occur near its marked peak, in April–May for Tmax and in May–June for Tmin, with very few heat waves in March and July. Essentially, using filtered temperatures tends to increase the heat wave temperature anomalies while using raw temperatures tends to increase the heat wave temperatures (see 15DW compared to NoFilter_15DW and the reference data compared to NoFilter in Figs. 4d,e,g,h); this demonstrates the result that there is no direct correspondence between the strongest intraseasonal and synoptic temperature fluctuations and the highest temperatures, the latter being more controlled by longer-term variability.

On average over the whole spring extended period, heat wave properties are not significantly sensitive to the chosen approach (see Table 1), except for temperature-related differences that are directly linked to the approach. Finally, the percentile based on a long fixed-window results

TABLE 1. Average heat wave properties obtained with our heat wave index using the BEST dataset over 1950–2012 (the reference data, first row), with other heat wave indices, and with our heat wave index using BEST, ERA-Interim, NCEP-2, and MERRA over 1979–2012. The first and second values in each cell correspond respectively to HWmax and HWmin properties. Boldface values indicate that they are significantly different (Student's *t* test at the 95% level) from those obtained in the reference; boldface and italic values indicate that they are significantly different from BEST over 1979–2012 and are used when comparing to various reanalyses (ERA-Interim, NCEP-2, and MERRA).

HWmax/HWmin	No. per year	Duration (day)	Area covered (%)	Tmax intensity (°C)	Tmin intensity (°C)	DTR (°C)	Tmax (°C)	Tmin (°C)
Reference	3.3/2.9	5.0/4.9	42.1/39.2	3.0/1.3	1.3/3.0	16.1/13.4	40.6/39.3	24.4/25.9
Comparison to other heat indices								
15DW	3.6/2.7	4.5/4.3	42.5/38.2	**2.9/1.6**	1.3/2.9	**15.6/12.6**	40.9/39.6	**25.2/27.0**
NoFilter_15DW	3.4/2.7	5.3/5.3	43.8/40.8	**2.4**/1.2	**1.1/2.3**	**15.5/12.4**	**41.5/40.1**	**25.9/27.7**
noFilter	3.6/2.9	**5.7**/5.6	**36.6/37.2**	**1.9/1.0**	**0.7/1.8**	16.0/**12.8**	**42.8/41.5**	**26.8/28.8**
Impact of the meteorological dataset on the detection								
BEST 1979–2012	3.5/2.5	5.1/5.4	41.9/40.9	3.0/1.5	1.5/***3.2***	16.0/13.3	41.0/39.7	25.0/26.4
ERA-Interim	***2.8***/2.2	5.0/6.3	***35.2/34.9***	***3.6***/1.3	1.5/***3.3***	***14.9/12.8***	***40.0/38.8***	25.1/26.0
NCEP-2	***2.1/1.6***	5.0/5.9	***31.1/32.4***	***4.6/0.5***	***0.4/6.2***	***19.1/10.3***	***39.6/37.5***	***20.5***/26.9
MERRA	***1.4***/2.4	5.1/***6.8***	***33.3/36.9***	***4.4/2.2***	***2.9***/3.2	***17.3/15.4***	***42.9/41.6***	25.5/26.2

in a steady seasonal distribution over the intensities, while the percentile based on a short moving window causes a steady seasonal distribution over the occurrence, with the possibility of having a wide range of heat wave intensities from extreme heat waves to less extreme warm spells. Thus the choice of approach used to detect a heat wave is important, and ideally it should be driven by the targeted questions and applications. For instance, our "meteorological" approach favors the selection of heat waves of close intensities (in terms of temperature anomaly), and this choice is well suited for further composite studies (Roehrig et al. 2011; Poan et al. 2013). The connectedness constraint should also be helpful for heat wave tracking analyses. More broadly, some applications in agricultural and health sectors may require additional information in the heat wave detection, for instance soil moisture, atmospheric humidity or apparent temperature [such as in the National Oceanic and Atmospheric Administration (NOAA) heat index, http://www.nws.noaa.gov/om/heat/heat_index.shtml], which are currently not taken into account in the indices discussed above.

b. *Sensitivity to the meteorological dataset*

For this study BEST is our reference dataset. In this section, the sensitivity of heat wave properties to the dataset is explored by applying the same methodology to three meteorological reanalyses, ERA-Interim, NCEP-2, and MERRA.

As the meteorological reanalyses only cover 1979–present, heat wave detection is restricted to their common period 1979–2012. BEST heat wave characteristics are very similar when detected over this shorter period (Fig. 5), with overall no significant difference at the 95% level for the mean morphological and temperature-related characteristics (except for a small increase of 0.2°C for HWmin Tmin anomalies).

The four products have distinct temperature distributions and annual cycles (see the appendix), which induces differences between heat wave properties detected with one or the other dataset. Their average properties are summarized in Table 1.

For HWmax events, the frequency of occurrence is slightly lower in ERA-Interim compared to BEST, and much lower in NCEP-2 and MERRA, by 40% and 60% respectively (Fig. 5a). In contrast, the frequency of occurrence of HWmin events is not significantly different between BEST, ERA-Interim, and MERRA. Nevertheless, all datasets capture the annual cycle of BEST heat wave frequency of occurrence documented above (i.e., that the further into the spring season, the smaller the probability of heat wave occurrence and the shorter these heat waves; not shown). Only ERA-Interim has a different behavior for HWmax events, which are most frequent in July. This appears to be linked to monthly differences in the temperature anomaly variances: indeed, for BEST, NCEP-2, and MERRA they slowly decrease from March to July whereas the ERA-Interim variances increase from June on (see the appendix).

The mean duration of HWmax events is similar in all reanalyses compared to BEST, in terms of distribution (Fig. 5b) and on average at the 95% level. HWmin events have a similar behavior except for MERRA events, which are overall longer.

Heat waves in the reanalyses cover smaller areas than in BEST by approximately 22×10^4 km^2 (Fig. 5c). BEST temperatures are constructed using a kriging regression method over station observations and are therefore quite sensitive to the density of the observational network.

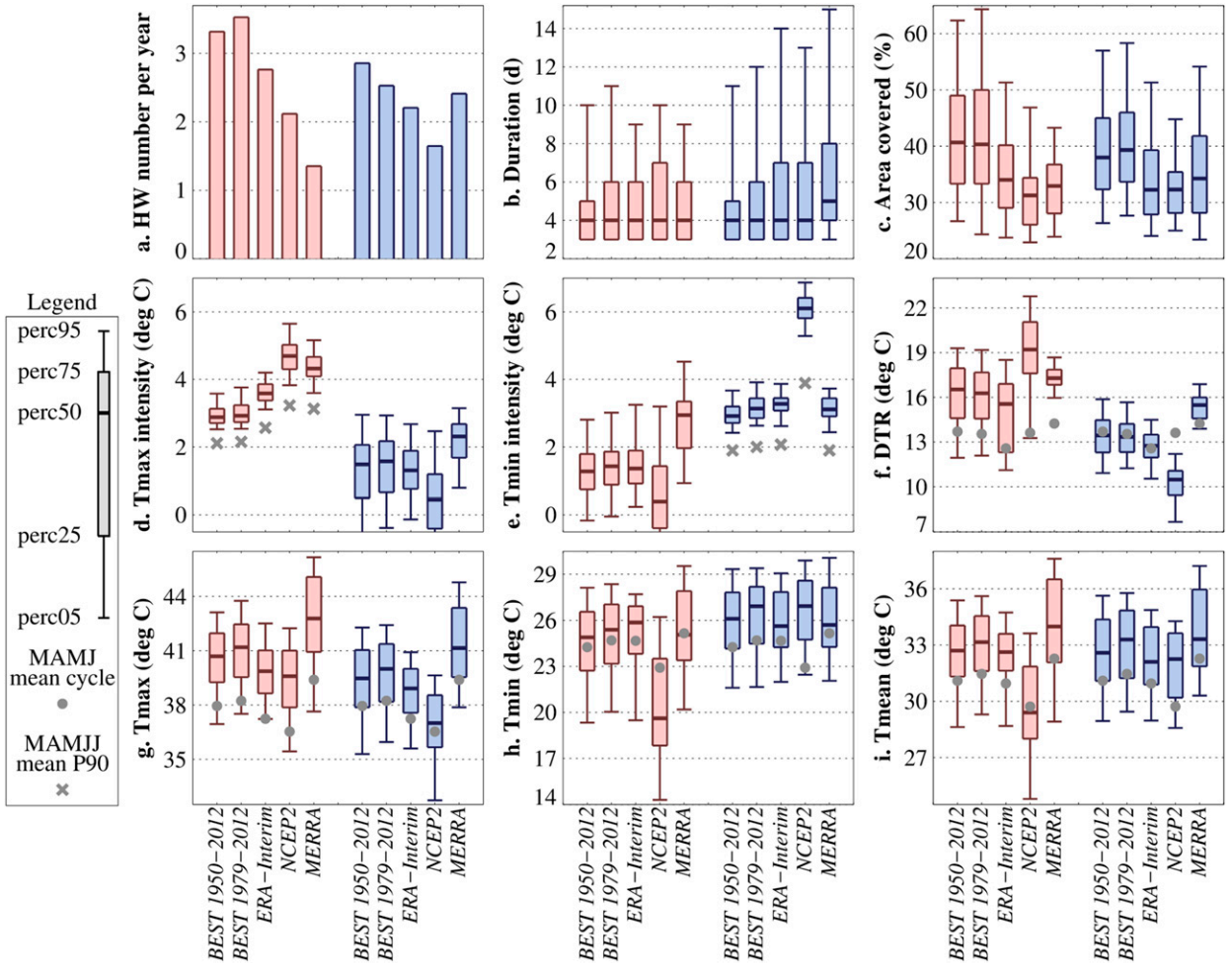

FIG. 5. As in Fig. 3, but over the whole period March–July for different meteorological products: BEST, ERA-Interim, NCEP-2, and MERRA over the period 1979–2012 unless indicated.

It is possible that the weak density of stations over the Sahel tends to smooth BEST temperatures (Rohde et al. 2013a). In contrast, reanalyses with their higher-resolution grids can generate smaller-scale structures, which are more likely to produce spatially smaller heat waves.

All reanalyses also simulate stronger HWmax events than BEST (Fig. 5d). Tmax anomalies of HWmax are 0.6°C higher in ERA-Interim and 1.5°C higher in NCEP-2 and MERRA. By contrast, Tmin anomalies of HWmin are rather consistent across the datasets, except for NCEP-2, which strongly overestimates their intensity (on average 6.2°C compared to roughly 3°C). This shift is in direct relation with the Tmin anomaly variance of NCEP-2, which reaches more than twice the variance of the other datasets (Figs. A1e and A2e).

The analysis of the temperature distribution discussed in the appendix indicates that NCEP-2 and ERA-Interim have a cold bias in Tmax while MERRA has a warm bias. NCEP-2 has a very strong Tmin bias (up to −3°C). As a result, heat wave temperatures mostly follow the dataset mean temperature biases (Figs. 5g–i), except for HWmin Tmin in NCEP-2 for which the cold bias is compensated by an overly strong high-frequency variability of Tmin.

In summary, heat wave characteristics are quite sensitive to the meteorological product used to detect them. The main differences seem to arise from the nature of the dataset considered (model versus interpolated local observations) and from the differently biased temperature background. The former affects heat wave size and duration while the latter drives differences in heat wave temperatures. Both the synoptic and intraseasonal variability of reanalyzed temperatures, especially for NCEP-2, affect the occurrence of the heat waves. Finally, our results show that care should be taken when choosing a dataset for heat wave studies, especially over regions where in situ observations are scarce, because differences between some basic heat waves

TABLE 2. As in Table 1, but for trends of the heat wave characteristics over March–July. A trend is considered nonsignificant (NS) if the p value is larger than 0.05.

		Number per year per decade	Duration (day decade^{-1})	Area covered (% decade^{-1})	Tmax intensity (°C decade^{-1})	Tmin intensity (°C decade^{-1})	DTR (°C decade^{-1})	Tmax (°C decade^{-1})	Tmin (°C decade^{-1})
Reference 1950–2012	HWmax	+0.22	NS	NS	NS	+0.13	−0.23	+0.27	+0.5
	HWmin	NS	NS	+0.98	+0.16	+0.05	NS	+0.35	+0.44
Comparison to other heat indices									
30Filter	HWmax	NS	NS	+1.1	+0.04	NS	NS	+0.23	+0.25
	HWmin	NS	NS	NS	NS	NS	NS	+0.28	+0.38
15DW	HWmax	NS	NS	NS	NS	+0.13	NS	+0.27	+0.35
	HWmin	NS	NS	NS	NS	NS	NS	+0.25	+0.28
NoFilter_15DW	HWmax	+0.92	+0.42	+1.37	NS	NS	−0.25	NS	+0.35
	HWmin	+1.12	NS	NS	NS	−0.16	NS	+0.30	+0.31
NoFilter	HWmax	+0.90	+0.42	NS	NS	NS	−0.28	NS	+0.33
	HWmin	+1.16	NS	+2.49	NS	−0.15	+0.15	NS	NS
Impact of the meteorological dataset on the detection									
BEST 1979–2012	HWmax	NS	NS	NS	NS	NS	NS	+0.40	NS
	HWmin	NS	NS	NS	NS	NS	NS	+0.55	NS
ERA-Interim	HWmax	−0.59	NS	NS	−0.12	NS	NS	NS	NS
	HWmin	NS	NS	NS	NS	NS	NS	NS	NS
NCEP-2	HWmax	NS	−0.89	NS	NS	NS	NS	+0.66	NS
	HWmin	NS	NS	−2.13	NS	NS	NS	NS	+0.78
MERRA	HWmax	NS	NS	NS	NS	−0.49	NS	+0.90	NS
	HWmin	NS	NS	−3.39	NS	−0.13	+0.26	+0.86	+0.60

characteristics can be quite large. Overall, ERA-Interim appears to be the best suited meteorological reanalysis to study heat waves when compared with local and gridded observations over the Sahel.

5. Long-term evolution of heat waves since 1950

Since 1950, temperatures have strongly increased in spring over the Sahel. In this section, we analyze the links between this climatic trend and heat wave trends, with two complementary approaches.

a. Event-based approach

The long-term linear trends (1950–2012) of the various heat wave properties are summarized in Table 2. HWmax event duration and area do not show any significant trend over the period, while their frequency of occurrence has slightly increased by 0.22 heat waves per decade. The area covered by HWmin events has significantly increased by 1% (3×10^4 km^2) per decade since 1950, while there are no significant trends for their frequency of occurrence and their duration. The HWmax and HWmin intensity, as measured by their respective temperature anomalies, do not show any significant or strong trend either. In contrast, heat wave mean minimum, maximum, and daily averaged temperatures significantly increased between 1950 and 2010, from 0.27° to 0.5°C decade^{-1} depending on the heat wave type or the considered temperature variable. Heat wave Tmin increased faster than the corresponding Tmax, about 0.5°C decade^{-1} for Tmin compared to roughly 0.3°C decade^{-1} for Tmax. The fact that Tmin increased faster than Tmax is consistent with the trends found by Guichard et al. (2015) in the Sahel. More broadly, this result has been highlighted worldwide and might be related for a part to an increase in the cloud cover (Karl et al. 1993; Easterling et al. 1997).

From 1950 to 2010, the long-term temperature trend over the Sahel is highly variable from month to month (Guichard et al. 2015). In April and May, monthly mean temperatures exhibit the most robust linear trend of around +0.3°C decade^{-1}, and these are also the hottest months of the year. Therefore, only April and May are considered here to compare heat wave temperature trends to the mean Sahelian trend. Figure 6 shows the time series of April–May minimum and maximum temperature trends over the Sahel domain and their counterparts for the detected heat waves. A linear regression indicates that Sahel April–May mean maximum temperatures trends are equal to +0.25° ± 0.09°C decade^{-1} (95% confidence level), while the minimum temperature trend reaches +0.32° ± 0.08°C decade^{-1}. Even though this is consistent with a mean temperature trend in April–May of 0.3°C decade^{-1}, this emphasizes different rates of increase for minimum and maximum temperature. HWmax event maximum temperatures mostly follow the

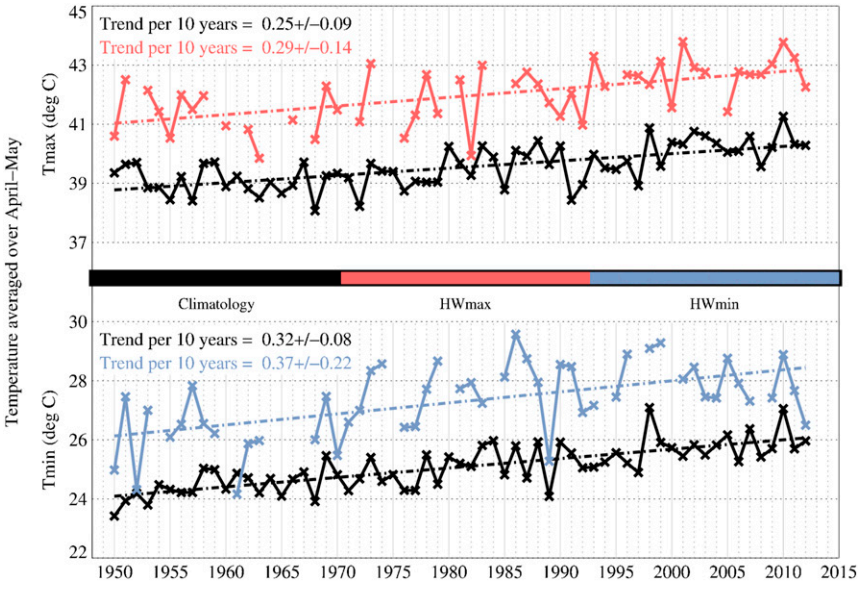

FIG. 6. Time series of April–May mean (top) Tmax and (bottom) Tmin for each year from 1950 to 2012 on average over the Sahelian domain (solid black) and over heat waves, namely (top) Tmax of HWmax (solid red) and (bottom) Tmin of Hwmin (solid blue); dotted–dashed lines correspond to the associated linear trends. Heat wave curves are discontinuous since heat waves do not occur every year. The Lagrangian approach is used to compute the heat wave trends.

increase of mean maximum temperature with a trend of $0.29° \pm 0.14°C\,decade^{-1}$, and HWmin event minimum temperatures evolve approximately at the same rate as mean minimum temperatures ($+0.37° \pm 0.22°C\,decade^{-1}$). Thus the long-term evolution of heat waves over the Sahel appears to be mainly driven by the background temperature trend. Changes in synoptic and intraseasonal variability, if any, do not significantly impact heat wave temperature trends.

The link between heat wave trends and regional or global temperature trends has been largely addressed in the literature. For instance, Russo et al. (2014) argued that the global surface area impacted by heat waves significantly increased in the last decades. Gershunov and Guirguis (2012) found positive trends of heat wave magnitudes over 1950–2012. They also reported that the California inland desert heat wave temperatures are increasing less rapidly than the mean temperature. Argüeso et al. (2016) showed that globally the mean climate warming is responsible for most of the heat wave changes in the next century except for Europe and North America, in agreement with Schoetter et al. (2015) for Europe. In the tropics, the climate warming is associated with a shift of the temperature distribution (Argüeso et al. 2016; Déqué et al. 2017), which is consistent with our results.

The linear trends over 1979–2012 of the four datasets (section 4b) are displayed in Table 2. The smaller number of heat waves, in addition to the reduced time period, is likely to increase the odds of a nonsignificant value, and the results must be taken with care. The main result is that, when significant, the Tmax, Tmean, and Tmin show a positive trend. Conversely, for HWmin, there is a significant diminution of the area covered when using NCEP-2 and MERRA. The spread of climatological trends estimated with these reanalyses is likely to be at play in the heat wave trends: Tmax climatological trends range from $+0.3°C\,decade^{-1}$ in ERA-Interim to $+0.55°C\,decade^{-1}$ in MERRA and Tmin trends from $+0.3°C\,decade^{-1}$ in MERRA to $+0.55°C\,decade^{-1}$ in NCEP-2 (Fig. A3).

The heat waves detected in the present work are Lagrangian objects and therefore the analysis of the trends of some of their properties raises some questions. In an environment with spatial temperature gradients, heat wave temperature trends could involve shifts in the areas impacted by the heat wave in association with possibly different climatological trends over these areas. It would thus depend on the spatial pattern of the mean Tmin and Tmax long-term changes, which are shown in Figs. 7a and 7b. Indeed, those climatological trends are spatially dependent (Guichard et al. 2012; Fontaine et al. 2013; Guichard et al. 2015; Moron et al. 2016): both Tmin and Tmax linear trends are higher over Mauritania, Mali, and northern and western Niger, and decrease to the south toward the Guinean coast and to the very east over Chad. Hence the spatial and temporal distribution of the heat waves can influence the above heat wave trends. To better assess the role of

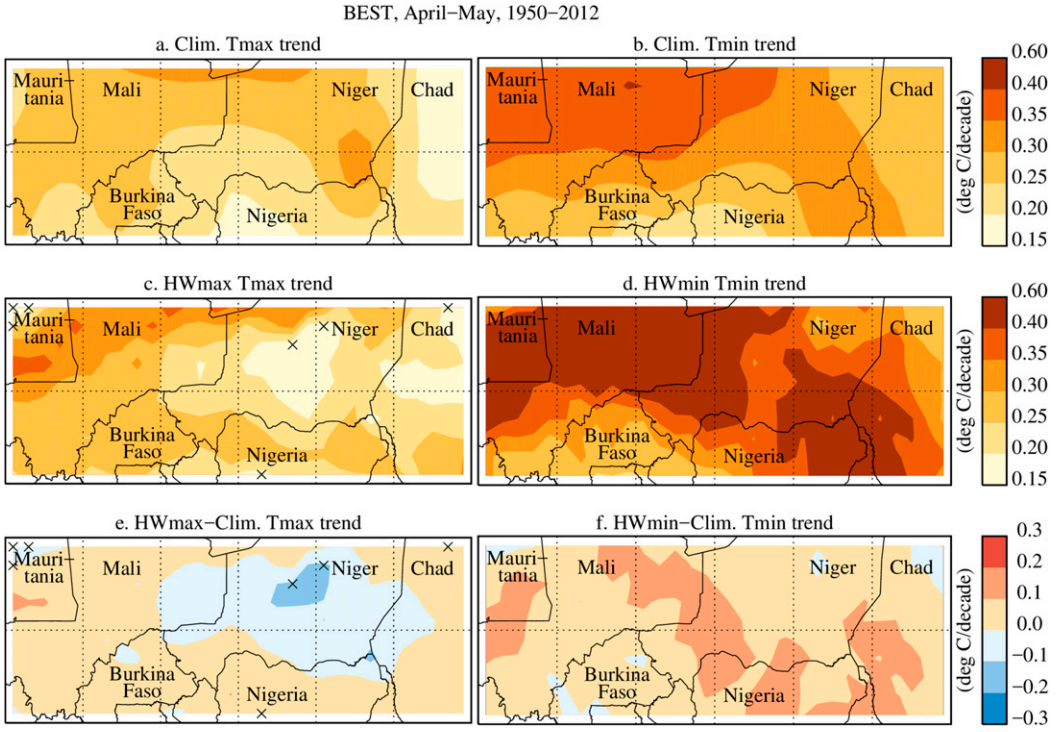

FIG. 7. Maps of climatological trends of (a) Tmax and (b) Tmin computed over April–May for 1950–2012; (c),(d) As in (a),(b), but for Tmax of HWmax heat waves and Tmin of HWmin heat waves, and (e),(f) the difference between climatological and heat wave trends [i.e., (e) = (c) − (a); (f) = (d) − (b)]. Crosses indicate grid points where differences are not significant at the 95% level.

these distributions, we weighted the climatological trend by the total number of heat wave days for each grid point (not shown): thus an area that is affected by a great number of heat wave days will contribute more than an area affected by a lower number. In practice HWmax and HWmin are located mostly in the eastern part of the Sahelian domain; however, the weighted climatological trends are unchanged. This nonhomogeneous spatial distribution of the heat waves can also be time dependent, so that heat wave temperature trends are then computed over slightly different climates. To avoid the issues linked to the Lagrangian approach, in the next section we investigate another option that uses a Eulerian approach to study the trends.

b. *Local Eulerian approach*

Trends can also be computed for each grid point, by considering the annual mean temperature for the days when heat waves occur at that grid point. The selection of heat waves over the Sahelian domain leads to retaining fewer heat waves at the edge of the Sahelian domain and thus the sample is substantially reduced. To avoid these edge effects, all heat waves detected over the whole African domain are accounted for, not only those overlapping over 20% of the Sahel domain. The maps of significant linear trends are shown in Figs. 7c and 7d.

The Tmin trend of HWmin events is mostly uniform over the Sahel, reaching $+0.4°C\,decade^{-1}$ (Fig. 7d). It is slightly lower over Burkina Faso and southern Mali as well as over northern Chad, where the trends there are below $+0.3°C\,decade^{-1}$. Overall Tmin trends of HWmin events are close to the climatological April–May trends, or slightly stronger, particularly over the southeast part of the Sahel (Fig. 7f): HWmin are thus warming at the same rate or slightly faster than the mean regional climate. The Tmax trend of HWmax events is maximum over Mauritania, northern Mali, and northern Niger, reaching $+0.4°C\,decade^{-1}$ (Fig. 7c). It is minimum over central Niger and central Chad. There the trend is slightly weaker than the mean long-term warming (Fig. 7e), which indicates that HWmax events intensify less quickly than the mean climate. This could be interpreted as a saturation effect for maximum temperatures whose distributions are negatively skewed (Figs. A1d and A2d) and that are already very high over the region during HWmax events (e.g., it could involve physical mechanisms operating in the surface energy balance at high temperature). Interestingly, a similar result was noted by Gershunov and Guirguis (2012) over the California desert.

The differences between heat wave and climate trends range between −0.2° and 0.2°C decade^{-1}, which is close to the confidence interval of the trends themselves. Therefore, temperature trends at the climate and heat wave scales over the Sahel are mostly similar, with some spatial particularities that need to be further assessed.

6. Conclusions

This paper introduces a new heat wave detection methodology that comprises four different steps: a temperature filtering to focus on specific temporal scales, the determination of a temperature extreme threshold based on a March–July window 90th percentile, the application of a spatiotemporal constraint, and finally the selection of a particular geographic domain.

The filtering process enables us to focus on a specific type of heat waves, without mixing different temporal scales. Here, we focused on heat waves of synoptic to intraseasonal scales and thus we decoupled heat wave events from the annual cycle and long-term temperature variabilities. The use of a fixed window provides information on the seasonal evolution of the heat wave occurrences. The spatiotemporal constraint selects spatially and temporally coherent heat waves (here they last at least 3 days and cover more than 60×10^4 km^2). The final step of selecting a particular domain allows this heat index to be used over any region.

This heat index was applied separately to daily maximum and minimum temperatures (Tmax and Tmin) of the observational-based BEST dataset. We found an average of 3.3 "Tmax heat waves" (HWmax) and 2.9 "Tmin heat waves" (HWmin) per year. Both types of heat waves last on average around 5 days, cover roughly 120×10^4 km^2 with a temperature anomaly of +3°C. In May, the mean Tmax (Tmin) of HWmax (HWmin) reaches up to 42°C (28°C) or more. The HWmin areas are slightly smaller than the HWmax. Concomitant HWmax and HWmin events happened only one-fifth of the time. This result supports the decision to separately analyze maximum and minimum temperatures in the Sahelian region.

Heat waves also become shorter and less frequent from March to July. HWmin events are particularly rare in June–July. In March–April, heat wave temperature anomalies are stronger than those in June–July, a consequence of the temperature anomaly variance distribution of BEST.

There was no strong climatological trend of heat wave occurrences over 1950–2012. However, their Tmax (Tmin) significantly increased from 1950 to 2012, by 1.6°C for HWmax (2.6°C for HWmin). This warming is consistent with a mean shift of the temperature distribution, in line with the results of Argüeso et al. (2016) in the tropics; the heat waves are not intrinsically hotter, but rather they reflect the warming climate. In the northern Sahel, however, we found that the climatic warming trend is stronger than the heat wave trend for the Tmax, as also highlighted by Gershunov and Guirguis (2012) over California deserts.

The results are quite similar when the percentile is computed over a 15-day moving window, except for differences over the seasonal occurrences that are directly linked to methodological choices. The constant percentile led to a steady temperature anomaly distribution throughout the season while the moving-window produced a steady seasonal occurrence distribution, leading to a wide range of heat wave intensities. Over a moving window without the filtering process, we found that heat waves were longer and larger. As expected, heat waves are also becoming more frequent by one per decade when raw instead of filtered temperature are used.

The heat index was also computed similarly with temperatures from three meteorological reanalyses, namely ERA-Interim, NCEP-2, and MERRA, over 1979–2012. The heat waves were smaller than for BEST; this could be related to the different nature of the datasets (observationally based versus model); the heat wave sizes in reanalyses are not smaller for the finer grid though. Inherent biases between the distributions of climatological means and variances resulted in significant differences in temperature-related heat wave characteristics. This notably affects Tmin anomalies in NCEP-2 HWmin (they are 3°C higher on average) and to a lesser extent Tmax in MERRA HWmax, while temperature and temperature anomalies in both heat wave types are much closer to BEST in ERA-Interim.

Perkins (2015) identified three potential drivers of heat waves: synoptic systems, soil moisture–atmosphere feedbacks, and larger-scale dynamics. Fontaine et al. (2013) studied the latter and suggested that Rossby waves may play a role in the forcing heat waves. The second potential driver is unlikely here since soil moisture is very low during springtime in the Sahel. However, this does not preclude the significance of other mechanisms of surface–atmosphere interaction in this region. For instance, Largeron et al. (2017, manuscript submitted to *Climate Dyn.*) recently described a major water vapor impact on nighttime temperature in a Sahelian heat wave case study.

More generally, further studies are necessary to analyze the meteorological situations associated with Sahelian heat waves and to understand how physical processes distinctly shape nighttime and daytime temperatures during these events. The present set of detected heat waves, combined with observations and dynamical fields from reanalyses, should be useful for such purpose. This would allow for studying composites of these events; for instance, at a given location we could

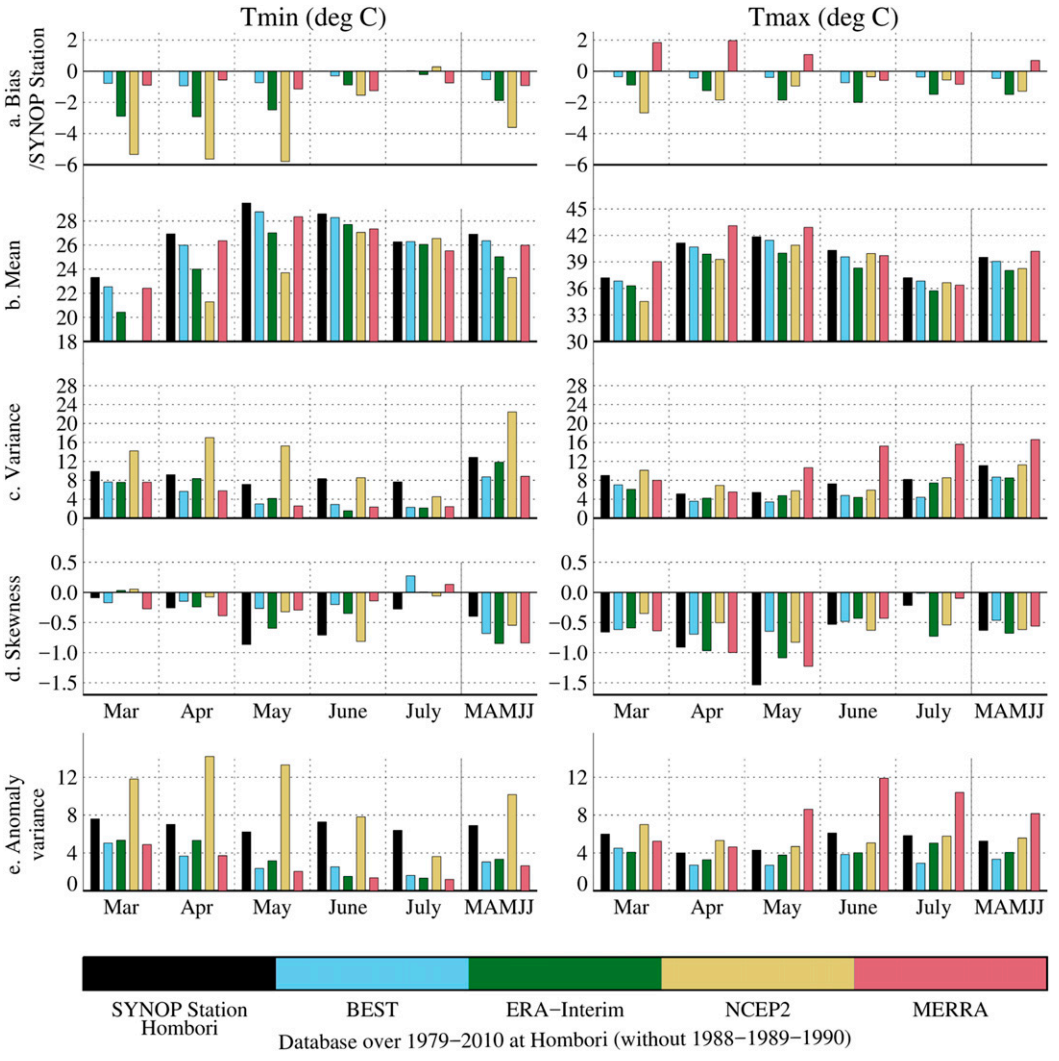

FIG. A1. Statistical moments of the (left) minimum and (right) maximum temperature distributions of the observationally gridded dataset BEST, the reanalyses ERA-Interim, NCEP-2, and MERRA, and the SYNOP station Hombori, Mali (15.33°N, 1.8°E), over 1979–2010 by month and over the March–July (MAMJJ) period: the differences between the mean of the gridded dataset and (a) the SYNOP observations, (b) the mean of the gridded dataset, (c) the variance, (d) the skewness, and (e) the anomaly variance. The climatic trends are removed before computing the moments. The anomaly variances in (e) correspond to the variance of the anomaly temperatures computed with the 90-day high-pass filter. The years 1988, 1989, and 1990 have been removed because of inconsistencies in the Tmin of Hombori.

define composites from the time sequences associated with the passages of heat waves. For the locations where in situ data are available [e.g., those from the African Monsoon Multidisciplinary Analysis–Couplage de l'Atmosphère Tropicale et du Cycle Hydrologique (AMMA-CATCH) network; Lebel et al. 2009], observations might also be used to analyze the dynamic and thermodynamic characteristics of the events at small scale.

Further studies should also investigate the causes behind the distinct trends in Tmax for HWmax and Tmin for HWmin. In particular, the strong Tmin trend raises questions about its potential links with changes in atmospheric water vapor or cloud cover (Karl et al. 1993; Easterling et al. 1997). Although observations are scarce, they are valuable for exploring relationships between water vapor and nighttime temperature during heat waves in a more systematic way (Evan et al. 2015).

Finally, from a modeling perspective, previous studies (e.g., Roehrig et al. 2013) point to a large spread in CMIP5 simulations of annual cycles and mean trends of temperatures over the Sahel. For heat waves specifically, our methodology applied to these simulations could document their ability to simulate heat waves. Moreover, as heat wave characteristics and trends may not be independent

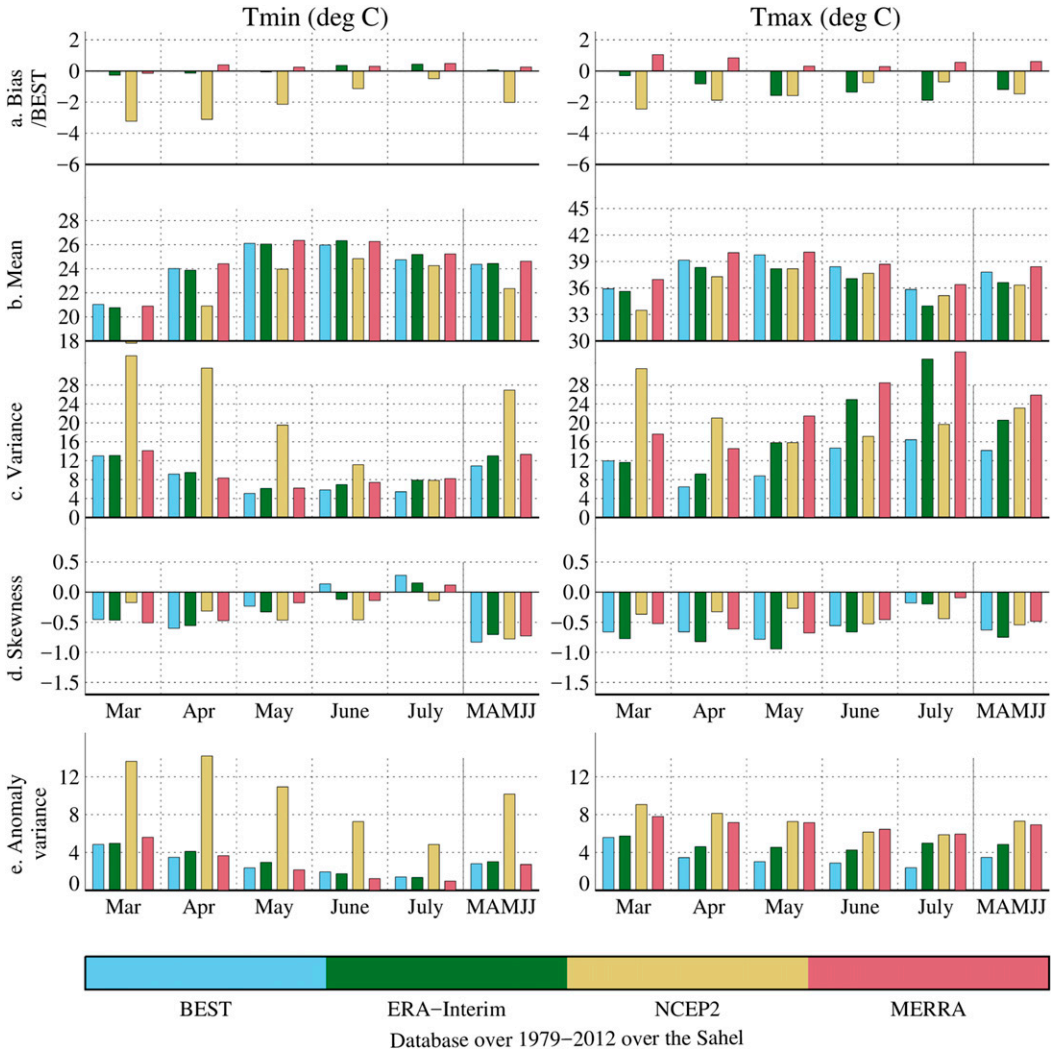

FIG. A2. As in Fig. A1, but for BEST, ERA-Interim, NCEP-2, and MERRA over the Sahelian domain (10°–20°N, 10°W–20°E) over 1979–2012. The climatological trends are removed before computing the moments.

from the simulated mean climate and climatological trends in the Sahel, it would be valuable to analyze their links.

Acknowledgments. This study is part of ANR project ACASIS (2014-2017, Grant ANR-13-SENV-0007). We thank the reviewers for their constructive comments and suggestions.

APPENDIX

Temperature Statistics and Climatological Trends among Datasets

The observational gridded product BEST and the three reanalyses ERA-Interim, NCEP-2 and MERRA were compared over 1979-2010 to two SYNOP stations with consistent temperature time series: Hombori (Guichard et al. 2015) and Niamey (Leauthaud et al. 2017). Figure A1 summarizes the main statistical characteristics of temperature distributions at Hombori or at the closest geographical point to this site for the datasets: the mean (Fig. A1b), the variance (Fig. A1c) and the skewness (Fig. A1d), as well as the differences between the mean of the gridded datasets and the SYNOP observations (Fig. A1a) for the maximum and minimum temperatures. The variance of the temperature anomalies are also displayed (Fig. A1e). The climatological trends were removed before computing those statistics.

First we compared their monthly values from March to July and their March–July average (Figs. A1a,b). BEST closely follows SYNOP data for both maximum and

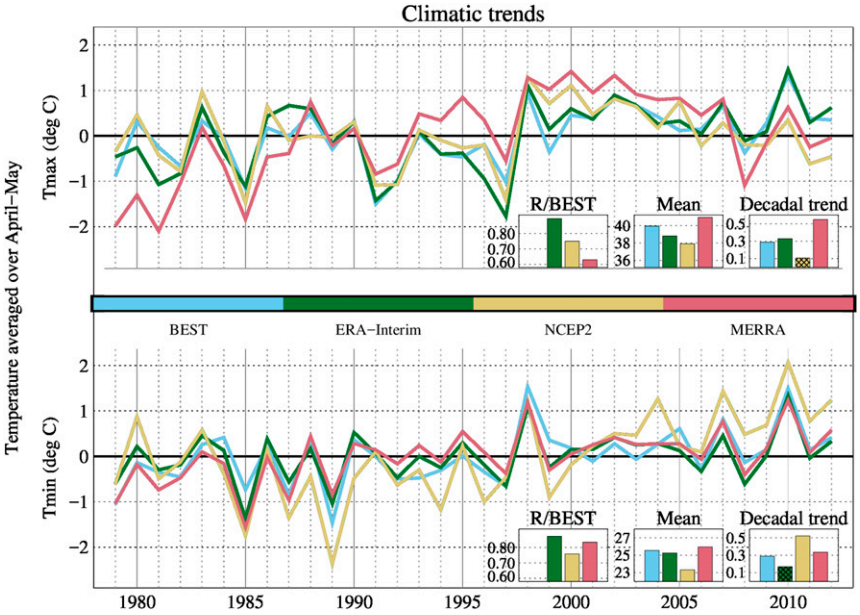

FIG. A3. Time series of Sahelian-mean Tmax and Tmin averaged over April–May. The correlation R between BEST and the datasets and the means (°C) and the linear trends (°C decade^{-1}) of the four datasets over April–May 1979–2012 are shown in the insets. Crosses indicate trends that are not significant at the 95% level.

minimum temperatures (Tmin and Tmax) whereas NCEP-2 displays a cold bias, more pronounced in the early season and much stronger for Tmin (reaching up to −6°C in May). The same behaviour is observed for ERA-Interim but to a lesser extent, with biases ranging from −1° to −3°C. On the contrary, in MERRA, while Tmin is close to SYNOP data, Tmax is globally higher by around +2°C in the early season. Figure A1b shows the seasonal cycle of temperature: the maxima of Tmax are in April and May for the SYNOP station, BEST, ERA-Interim and MERRA while they are shifted to May and June for NCEP-2. The maxima of Tmin are in May and June for all except NCEP-2 which are again shifted later in the season, over June–July. The spreads of the distributions are quantified in Figs A1c,e with the variance. Overall the reanalyses and BEST display a lower variance values than the SYNOP data. However, NCEP-2 stands out for the Tmin anomalies with variances that are up to twice higher than in SYNOP data, and MERRA for the Tmax with also twice the variance of SYNOP data over May, June, and July (Fig. A1e). The seasonal-mean variance is also higher due to this behavior during these last three months. The skewness, which measures asymmetry of the distribution, is shown in Fig. A1d. Overall the skewness of all distributions are negative, i.e. the distribution are skewed to the left, more strongly for Tmax than for Tmin, and more so for SYNOP data.

A similar analysis has been performed over Niamey (not shown) and over the Sahelian domain (Fig. A2). The bias of the latter are computed as differences from BEST temperatures which were the closest to SYNOP temperatures. The conclusions are similar except for the biases and the Tmax anomaly variances: for Tmin, the biases of ERA-Interim are closer to −1°C than −3°C at Niamey and there are no biases on average over the Sahel (Fig. A2a). The variance of Tmax anomalies on average over the Sahel are decreasing from March to July, except for ERA-Interim values that are higher in July than in May–June (Fig. A2e). Finally, as may be expected BEST is the closest to SYNOP data in terms of mean, seasonal cycle, variance and skewness. On average, NCEP-2 temperature is too low (for both Tmin and Tmax), this is also the case for Tmax in ERA-Interim while MERRA Tmax is too high. NCEP-2 seasonal maximum occurs one month too late and it exhibits a much higher variance of Tmin anomalies. The same applies for Tmax anomalies in MERRA.

The time series of Tmax and Tmin on average over the Sahel over April–May from 1979 to 2012 are displayed in Fig. A3 for BEST and the three reanalyses. Correlations R between BEST and the datasets, the means and the linear trends (°C decade^{-1}) are shown in the insets. Overall, ERA-Interim values are the closest to BEST values, with correlations R higher than 0.8 for both Tmax and Tmin. The reanalyses reproduce relatively

well the distinct year-to-year fluctuations of Tmin and Tmax, but the trends in Tmin and Tmax, both on the order of 0.3°C decade^{-1} are not as well captured. In particular, the trend in Tmin is too low in ERA-Interim, and strongly overestimated in NCEP-2, while the trend in Tmax is too high is MERRA and too low in NCEP-2.

REFERENCES

Ali, A., T. Lebel, and A. Amani, 2003: Invariance in the spatial structure of Sahelian rain fields at climatological scales. *J. Hydrometeor.*, **4**, 996–1011, doi:10.1175/1525-7541(2003)004<0996:IITSSO>2.0.CO;2.

Argüeso, D., A. Di Luca, S. E. Perkins-Kirkpatrick, and J. P. Evans, 2016: Seasonal mean temperature changes control future heat waves. *Geophys. Res. Lett.*, **43**, 7653–7660, doi:10.1002/2016GL069408.

Azongo, D. K., T. Awine, G. Wak, F. N. Binka, and A. R. Oduro, 2012: A time series analysis of weather variability and all-cause mortality in the Kasena-Nankana districts of northern Ghana, 1995–2010. *Global Health Action*, **5**, 14–22, doi:10.3402/gha.v5i0.19073.

Basu, R., and J. M. Samet, 2002: Relation between elevated ambient temperature and mortality: A review of the epidemiologic evidence. *Epidemiol. Rev.*, **24**, 190–202, doi:10.1093/epirev/mxf007.

Coumou, D., and S. Rahmstorf, 2012: A decade of weather extremes. *Nat. Climate Change*, **2**, 491–496, doi:10.1038/nclimate1452.

Cowan, T., A. Purich, S. Perkins, A. Pezza, G. Boschat, and K. Sadler, 2014: More frequent, longer, and hotter heat waves for Australia in the twenty-first century. *J. Climate*, **27**, 5851–5871, doi:10.1175/JCLI-D-14-00092.1.

Dee, D. P., and Coauthors, 2011: The ERA-Interim reanalysis: Configuration and performance of the data assimilation system. *Quart. J. Roy. Meteor. Soc.*, **137**, 553–597, doi:10.1002/qj.828.

Déqué, M., S. Calmanti, O. B. Christensen, A. Dell Aquila, C. F. Maule, A. Haensler, G. Nikulin, and C. Teichmann, 2017: A multi-model climate response over tropical Africa at +2°C. *Climate Serv.*, **7**, 87–95, doi:10.1016/j.cliser.2016.06.002.

Diboulo, E., A. Sié, J. Rocklöv, L. Niamba, M. Yé, C. Bagagnan, and R. Sauerborn, 2012: Weather and mortality: A 10 year retrospective analysis of the Nouna Health and Demographic Surveillance System, Burkina Faso. *Global Health Action*, **5**, 6–13, doi:10.3402/gha.v5i0.19078.

Easterling, D. R., and Coauthors, 1997: Maximum and minimum temperature trends for the globe. *Science*, **277**, 364–367, doi:10.1126/science.277.5324.364.

Evan, A. T., C. Flamant, C. Lavaysse, C. Kocha, and A. Saci, 2015: Water vapor–forced greenhouse warming over the Sahara Desert and the recent recovery from the Sahelian drought. *J. Climate*, **28**, 108–123, doi:10.1175/JCLI-D-14-00039.1.

Fiolleau, T., and R. Roca, 2013: An algorithm for the detection and tracking of tropical mesoscale convective systems using infrared images from geostationary satellite. *IEEE Trans. Geosci. Remote Sens.*, **51**, 4302–4315, doi:10.1109/TGRS.2012.2227762.

Fischer, E. M., and C. Schär, 2010: Consistent geographical patterns of changes in high-impact European heatwaves. *Nat. Geosci.*, **3**, 398–403, doi:10.1038/ngeo866.

Fitzpatrick, R. G. J., C. L. Bain, P. Knippertz, J. H. Marsham, and D. J. Parker, 2015: The West African monsoon onset: A concise comparison of definitions. *J. Climate*, **28**, 8673–8694, doi:10.1175/JCLI-D-15-0265.1.

Fontaine, B., S. Janicot, and P.-A. Monerie, 2013: Recent changes in air temperature, heat waves occurrences, and atmospheric circulation in northern Africa. *J. Geophys. Res. Atmos.*, **118**, 8536–8552, doi:10.1002/jgrd.50667.

Frappart, F., and Coauthors, 2009: Rainfall regime across the Sahel band in the Gourma region, Mali. *J. Hydrol.*, **375**, 128–142, doi:10.1016/j.jhydrol.2009.03.007.

Garenne, M., 2016: La pression de la population dans les Pays Sahéliens Francophones: Analyse des estimations et projections de population 1950–2100. Ferdi Working Paper 168, 26 pp., http://www.ferdi.fr/sites/www.ferdi.fr/files/publication/fichiers/p168_-ferdi-_michel_garenne.pdf.

Gershunov, A., and K. Guirguis, 2012: California heat waves in the present and future. *Geophys. Res. Lett.*, **39**, L18710, doi:10.1029/2012GL052979.

Gounou, A., F. Guichard, and F. Couvreux, 2012: Observations of diurnal cycles over a West African meridional transect: Pre-monsoon and full-monsoon seasons. *Bound.-Layer Meteor.*, **144**, 329–357, doi:10.1007/s10546-012-9723-8.

Guichard, F., L. Kergoat, E. Mougin, F. Timouk, F. Baup, P. Hiernaux, and F. Lavenu, 2009: Surface thermodynamics and radiative budget in the Sahelian Gourma: Seasonal and diurnal cycles. *J. Hydrol.*, **375**, 161–177, doi:10.1016/j.jhydrol.2008.09.007.

——, ——, ——, and F. Hourdin, 2012: The annual cycle of temperature in the Sahel and its climatic sensitivity. *2012 Fall Meeting*, San Francisco, CA, Amer. Geophys. Union, Abstract GC33A-1004.

——, ——, F. Hourdin, C. Léauthaud, J. Barbier, E. Mougin, and B. Diarra, 2015: Le réchauffement climatique observé depuis 1950 au Sahel in "Evolutions récentes et futures du climat en Afrique de l'Ouest : Evidences, incertitudes et perceptions." *Les Sociétés Rurales Face aux Changements Climatiques et Environnementaux en Afrique de l'Ouest*, B. Sultan et al., Eds., IRD, 23–42.

Ito, H., N. C. Johnson, and S.-P. Xie, 2013: Subseasonal and interannual temperature variability in relation to extreme temperature occurrence over East Asia. *J. Climate*, **26**, 9026–9042, doi:10.1175/JCLI-D-12-00676.1.

Janicot, S., and Coauthors, 2011: Intraseasonal variability of the West African monsoon. *Atmos. Sci. Lett.*, **12**, 58–66, doi:10.1002/asl.280.

Kanamitsu, M., W. Ebisuzaki, J. Woollen, S.-K. Yang, J. J. Hnilo, M. Fiorino, and G. L. Potter, 2002: NCEP–DOE AMIP-II Reanalysis (R-2). *Bull. Amer. Meteor. Soc.*, **83**, 1631–1643, doi:10.1175/BAMS-83-11-1631.

Karl, T. R., and Coauthors, 1993: A new perspective on recent global warming: Asymmetric trends of daily maximum and minimum temperature. *Bull. Amer. Meteor. Soc.*, **74**, 1007–1023, doi:10.1175/1520-0477(1993)074<1007:ANPORG>2.0.CO;2.

Knippertz, P., and A. H. Fink, 2006: Synoptic and dynamic aspects of an extreme springtime Saharan dust outbreak. *Quart. J. Roy. Meteor. Soc.*, **132**, 1153–1177, doi:10.1256/qj.05.109.

Kohler, M., N. Kalthoff, and C. Kottmeier, 2010: The impact of soil moisture modifications on CBL characteristics in West Africa: A case-study from the AMMA campaign. *Quart. J. Roy. Meteor. Soc.*, **136**, 442–455, doi:10.1002/qj.430.

Kovats, R. S., and S. Hajat, 2008: Heat stress and public health: A critical review. *Annu. Rev. Public Health*, **29**, 41–55, doi:10.1146/annurev.publhealth.29.020907.090843.

Leauthaud, C., and Coauthors, 2017: A 60-year reconstructed high-resolution local meteorological data set in central Sahel (1950–2009): Evaluation, analysis and application to land surface modelling. *Int. J. Climatol.*, **37**, 2699–2718, doi:10.1002/joc.4874.

Lebel, T., and Coauthors, 2009: AMMA-CATCH studies in the Sahelian region of West-Africa: An overview. *J. Hydrol.*, **375**, 3–13, doi:10.1016/j.jhydrol.2009.03.020.

Lee, W.-S., and M.-I. Lee, 2016: Interannual variability of heat waves in South Korea and their connection with large-scale atmospheric circulation patterns. *Int. J. Climatol.*, **36**, 4815–4830, doi:10.1002/joc.4671.

Lélé, M. I., and P. J. Lamb, 2010: Variability of the Intertropical Front (ITF) and rainfall over the West African Sudan–Sahel zone. *J. Climate*, **23**, 3984–4004, doi:10.1175/2010JCLI3277.1.

Lohou, F., and Coauthors, 2014: Surface response to rain events throughout the West African monsoon. *Atmos. Chem. Phys.*, **14**, 3883–3898, doi:10.5194/acp-14-3883-2014.

McMichael, A. J., and E. Lindgren, 2011: Climate change: Present and future risks to health, and necessary responses. *J. Intern. Med.*, **270**, 401–413, doi:10.1111/j.1365-2796.2011.02415.x.

Meehl, G. A., and C. Tebaldi, 2004: More intense, more frequent, and longer lasting heat waves in the 21st century. *Science*, **305**, 994–997, doi:10.1126/science.1098704.

Mora, C., and Coauthors, 2017: Global risk of deadly heat. *Nat. Climate Change*, **7**, 501–506, doi:10.1038/nclimate3322.

Moron, V., B. Oueslati, B. Pohl, S. Rome, and S. Janicot, 2016: Trends of mean temperatures and warm extremes in northern tropical Africa (1961–2014) from observed and PPCA-reconstructed time series. *J. Geophys. Res. Atmos.*, **121**, 5298–5319, doi:10.1002/2015JD024303.

Mutiibwa, D., S. J. Vavrus, S. A. McAfee, and T. P. Albright, 2015: Recent spatiotemporal patterns in temperature extremes across conterminous United States. *J. Geophys. Res. Atmos.*, **120**, 7378–7392, doi:10.1002/2015JD023598.

Nairn, J. R., and R. Fawcett, 2013: Defining heatwaves: Heatwave defined as a heat-impact event servicing all community and business sectors in Australia. Centre for Australian Weather and Climate Research Tech. Rep. CAWCR/TR-60, 85 pp., http://cawcr.gov.au/technical-reports/CTR_060.pdf.

Ouzeau, G., J.-M. Soubeyroux, M. Schneider, R. Vautard, and S. Planton, 2016: Heat waves analysis over France in present and future climate: Application of a new method on the EURO-CORDEX ensemble. *Climate Serv.*, **4**, 1–12, doi:10.1016/j.cliser.2016.09.002.

Perkins, S. E., 2015: A review on the scientific understanding of heatwaves—Their measurement, driving mechanisms, and changes at the global scale. *Atmos. Res.*, **164–165**, 242–267, doi:10.1016/j.atmosres.2015.05.014.

——, and L. V. Alexander, 2013: On the measurement of heat waves. *J. Climate*, **26**, 4500–4517, doi:10.1175/JCLI-D-12-00383.1.

——, ——, and J. R. Nairn, 2012: Increasing frequency, intensity and duration of observed global heatwaves and warm spells. *Geophys. Res. Lett.*, **39**, L20714, doi:10.1029/2012GL053361.

Petrou, M., and P. Bosdogianni, 2004: *Image Processing: The Fundamentals.* John Wiley and Sons, 333 pp.

Poan, D. E., R. Roehrig, F. Couvreux, and J.-P. Lafore, 2013: West African monsoon intraseasonal variability: A precipitable water perspective. *J. Atmos. Sci.*, **70**, 1035–1052, doi:10.1175/JAS-D-12-087.1.

Rienecker, M. M., and Coauthors, 2011: MERRA: NASA's Modern-Era Retrospective Analysis for Research and Applications. *J. Climate*, **24**, 3624–3648, doi:10.1175/JCLI-D-11-00015.1.

Robinson, P. J., 2001: On the definition of a heat wave. *J. Appl. Meteor.*, **40**, 762–775, doi:10.1175/1520-0450(2001)040<0762:OTDOAH>2.0.CO;2.

Roehrig, R., F. Chauvin, and J.-P. Lafore, 2011: 10–25-day intraseasonal variability of convection over the Sahel: A role of the Saharan heat low and midlatitudes. *J. Climate*, **24**, 5863–5878, doi:10.1175/2011JCLI3960.1.

——, D. Bouniol, F. Guichard, F. Hourdin, and J.-L. Redelsperger, 2013: The present and future of the West African monsoon: A process-oriented assessment of CMIP5 simulations along the AMMA transect. *J. Climate*, **26**, 6471–6505, doi:10.1175/JCLI-D-12-00505.1.

Rohde, R., and Coauthors, 2013a: Berkeley Earth temperature averaging process. *Geoinf. Geostat. Overview*, **1**, doi:10.4172/2327-4581.1000103.

——, and Coauthors, 2013b: A new estimate of the average Earth surface land temperature spanning 1753 to 2011. *Geoinf. Geostat. Overview*, **1**, doi:10.4172/2327-4581.1000101.

Russo, S., and Coauthors, 2014: Magnitude of extreme heat waves in present climate and their projection in a warming world. *J. Geophys. Res. Atmos.*, **119**, 12 500–12 512, doi:10.1002/2014JD022098.

Schoetter, R., J. Cattiaux, and H. Douville, 2015: Changes of western European heat wave characteristics projected by the CMIP5 ensemble. *Climate Dyn.*, **45**, 1601–1616, doi:10.1007/s00382-014-2434-8.

Schwendike, J., N. Kalthoff, and M. Kohler, 2010: The impact of mesoscale convective systems on the surface and boundary-layer structure in West Africa: Case-studies from the AMMA campaign 2006. *Quart. J. Roy. Meteor. Soc.*, **136**, 566–582, doi:10.1002/qj.599.

Sheehy, J. E., A. Elmido, G. Centeno, and P. Pablico, 2005: Searching for new plants for climate change. *J. Agric. Meteor.* **60**, 463–468, doi:10.2480/agrmet.463.

Sivakumar, M. V. K., 1992: Empirical analysis of dry spells for agricultural applications in West Africa. *J. Climate*, **5**, 532–539, doi:10.1175/1520-0442(1992)005<0532:EAODSF>2.0.CO;2.

Slingo, A., H. E. White, N. A. Bharmal, and G. J. Robinson, 2009: Overview of observations from the RADAGAST experiment in Niamey, Niger: 2. Radiative fluxes and divergences. *J. Geophys. Res.*, **114**, D00E04, doi:10.1029/2008JD010497.

Stefanon, M., F. D'Andrea, and P. Drobinski, 2012: Heatwave classification over Europe and the Mediterranean region. *Environ. Res. Lett.*, **7**, 014023, doi:10.1088/1748-9326/7/1/014023.

Sultan, B., S. Janicot, and A. Diedhiou, 2003: The West African monsoon dynamics. Part I: Documentation of intraseasonal variability. *J. Climate*, **16**, 3389–3406, doi:10.1175/1520-0442(2003)016<3389:TWAMDP>2.0.CO;2.

——, and Coauthors, 2013: Assessing climate change impacts on sorghum and millet yields in the Sudanian and Sahelian savannas of West Africa. *Environ. Res. Lett.*, **8**, 014040, doi:10.1088/1748-9326/8/1/014040.

United Nations Department of Economic and Social Affairs: Population Division, 2017: World population prospects: The 2017 revision, key findings and advance tables. UN Working Paper ESA/P/WP/248, 53 pp., https://esa.un.org/unpd/wpp/Publications/Files/WPP2017_KeyFindings.pdf.

Vizy, E. K., and K. H. Cook, 2009: A mechanism for African monsoon breaks: Mediterranean cold air surges. *J. Geophys. Res.*, **114**, D01104, doi:10.1029/2008JD010654.

Willett, K. M., and S. Sherwood, 2012: Exceedance of heat index thresholds for 15 regions under a warming climate using the wet-bulb globe temperature. *Int. J. Climatol.*, **32**, 161–177, doi:10.1002/joc.2257.

Zhang, X., L. Alexander, G. C. Hegerl, P. Jones, A. K. Tank, T. C. Peterson, B. Trewin, and F. W. Zwiers, 2011: Indices for monitoring changes in extremes based on daily temperature and precipitation data. *Wiley Interdiscip. Rev.: Climate Change*, **2**, 851–870, doi:10.1002/wcc.147.